Atmospheric Environment 271 (2022) 118898

Contents lists available at ScienceDirect

Atmospheric Environment

journal homepage: www.elsevier.com/locate/atmosenv

Performance comparison of Fengyun-4A and Himawari-8 in $PM_{2.5}$ estimation in China

Yuqing Hu [a], Chao Zeng [a,*], Tongwen Li [d], Huanfeng Shen [a,b,c]

[a] School of Resource and Environmental Sciences, Wuhan University, Wuhan, 430079, China
[b] Collaborative Innovation Center of Geospatial Technology, Wuhan, 430079, China
[c] The Key Laboratory of Geographic Information System, Ministry of Education, Wuhan University, Wuhan, 430079, China
[d] School of Geospatial Engineering and Science, Sun Yat-Sen University, Zhuhai, 519082, China

HIGHLIGHTS

- Compared with the Himawari-8 satellite, Fengyun-4A satellite is more suitable for estimating $PM_{2.5}$ concentrations in China.
- Three different ten-fold cross-validation approaches are introduced for a comprehensive evaluation of two satellites.
- The spatial resolution and training data bring effects on the mappings, the effect of the platforms and retrieval algorithms can be ignored.

GRAPHICAL ABSTRACT

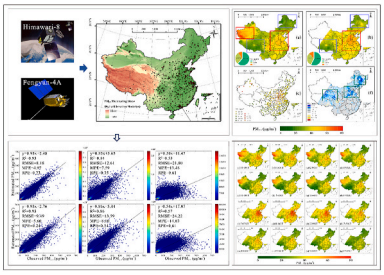

ARTICLE INFO

Keywords:
Air pollution
Geostationary satellite
FY-4A
Himawari-8
$PM_{2.5}$

ABSTRACT

The increase in the $PM_{2.5}$ concentration has become the focus of public concern due to the health risks it poses. In contrast to the sparsely distributed ground stations, geostationary satellites can provide a unique method of frequently monitoring national-scale $PM_{2.5}$ concentrations. The Himawari-8 and Fengyun-4A (FY-4A) satellites have both been used to monitor $PM_{2.5}$ concentrations due to their high spatial (5 km and 4 km, respectively) and temporal resolutions (hourly), but it is still not clear which satellite is more suitable for such studies. In this study, the hourly $PM_{2.5}$ concentrations were estimated based on a deep belief network using top-of-atmosphere (TOA) reflectance data and other auxiliary variables from April 2018 to March 2019. To comprehensively and effectively verify the accuracy of the results, three cross-validation methods were applied. The evaluation indexes of FY-4A were slightly higher than those of Himawari-8. The distributions of their estimated $PM_{2.5}$ concentration mappings were consistent in terms of the overall trend, but they exhibit regional inconsistencies. In-depth analysis of the results revealed that the main reasons for these inconsistencies are the differences in the spatial resolution, training data, satellite platforms, and retrieval algorithms. Through comparative analysis, the effects of the satellite platforms and retrieval algorithms were determined to be negligible. In general, the FY-4A satellite was found to be more adaptable to $PM_{2.5}$ concentration estimation in China due to its wide coverage and high estimation accuracy.

* Corresponding author.
E-mail addresses: zengchao@whu.edu.cn, zengchaozc@hotmail.com (C. Zeng).

https://doi.org/10.1016/j.atmosenv.2021.118898
Received 7 August 2021; Received in revised form 24 November 2021; Accepted 10 December 2021
Available online 17 December 2021

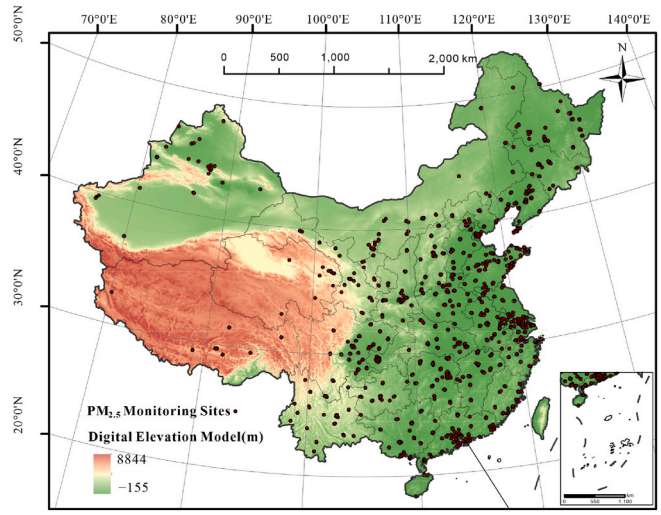

Fig. 1. Study Area and spatial distribution of $PM_{2.5}$ concentration stations.

1. Introduction

Fine particulate matter ($PM_{2.5}$) is an important index reflecting the degree of air pollution (Ma et al., 2016; Yu et al., 2017). In the past 10 years, with the rapid development of industrialization and urbanization, China has faced very serious air pollution problems (Sun et al., 2016; Guo et al., 2017; Song et al., 2019a). Many studies have shown that $PM_{2.5}$ concentrations can exacerbate respiratory diseases and significantly damage human health (Peng et al., 2009; Brauer et al., 2012; Bartell et al., 2013; Cohen et al., 2017; Xue et al., 2019). $PM_{2.5}$ also has serious negative impacts on the atmospheric environment (Koren et al., 2014; Seinfeld et al., 2016; Vu et al., 2019). Therefore, it is necessary to monitor the ground-level $PM_{2.5}$ concentrations to support the formulation of environmental governance policies.

The traditional $PM_{2.5}$ monitoring method directly obtains the $PM_{2.5}$ concentration values through ground monitoring stations with a high accuracy. However, sparse and uneven ground-level $PM_{2.5}$ concentration monitoring networks have limitations in terms of obtaining spatial information (Kloog et al., 2012; Yang et al., 2019). With the development of remote sensing technology, satellite data have been increasingly used to estimate surface $PM_{2.5}$ concentrations due to the wide coverage of the satellites (Zou et al., 2016; Li et al., 2017a). These satellites can be specifically divided into polar orbiting and geostationary satellites. Polar orbiting satellites have been most commonly used in previous studies. The results of these studies generally have a coarse temporal resolution (daily), which limits their application to air pollution research (Hu et al., 2014b; Liu et al., 2019b). A $PM_{2.5}$ concentration distribution with a fine temporal resolution is difficult to obtain (Hu et al., 2014a; Lary et al., 2015; Li et al., 2016; Singh et al., 2017; Sorek-Hamer et al., 2017). Therefore, geostationary satellites have become an indispensable tool for meteorological and land observations. For example, the Japan Meteorological Agency successfully launched an advanced geostationary satellite named Himawari-8 on October 7, 2014. As an important sensor on Himawari-8, the Advanced Himawari Imager (AHI) provides a spectral reflectance measurement every 10 min (Gupta et al., 2019). Fengyun-4A (FY-4A), which is the new generation of geostationary meteorological satellite developed by China, was launched on December 11, 2016. The FY-4A imager provides a full-disk scan every 15 min (Yang et al., 2017). These satellites provide a unique opportunity for high frequency $PM_{2.5}$ concentration retrieval.

Satellite observation data cannot be used to directly observe the atmospheric composition, so it is necessary to establish a non-linear relationship between the influencing factors. Many previous studies have shown that the aerosol optical depth (AOD) can be used to retrieve the $PM_{2.5}$ concentration. Satellite-derived AOD products have been extensively used for $PM_{2.5}$ concentration estimation (Levy et al., 2013; Song et al., 2014; Fang et al., 2016; Li et al., 2017b; Sarafian et al., 2019; Guo et al., 2021; Sun et al., 2021). However, AOD products have limitations in terms of their spatial coverage and inversion algorithms (Song et al., 2019b; Wang et al., 2019). Shen et al. (2018) proposed that the $PM_{2.5}$ concentration can be directly retrieved from top-of-atmosphere (TOA) reflectance data instead of AOD data (referred to as Ref-$PM_{2.5}$ modeling), which avoids intermediate errors, and they demonstrated that the Ref-$PM_{2.5}$ model preformed slightly better than the AOD-$PM_{2.5}$ model. Therefore, many researchers have recently started to utilize the Ref-$PM_{2.5}$ model to estimate and analyze $PM_{2.5}$ concentrations. For example, Liu et al. (2019a) retrieved $PM_{2.5}$ concentrations from the Himawari Imager satellite measured TOA reflectance data, and the performance was satisfactory on different temporal scales. Wang et al. (2021) set the Himawari-8 TOA reflectance, meteorological data, and NDVI as the input data to predict the hourly $PM_{2.5}$ concentrations in the Wuhan Urban Agglomeration. The model also performed well in Ref-$PM_{2.5}$ modeling. Comparing the two satellites, FY-4A's spatial resolution is higher than that of Himawari-8, and the coverage of FY-4A is larger than that of Himawari-8 in China. Many studies have used Himawari-8 reflectance data, but few have used FY-4A reflectance data.

Therefore, in this study, FY-4A and Himawari-8 satellites' TOA reflectance data were used in combination with auxiliary data to estimate the $PM_{2.5}$ concentration in China. The study gave some suggestions about which one was more suitable for estimating $PM_{2.5}$ concentration in China. Three cross-validation (CV) methods were introduced, including a new CV method that considers the uneven spatial distribution of the monitoring stations (denoted as SDCV). The results reveal the changes in the hour-level spatial distribution of the $PM_{2.5}$ concentration in China. The reasons for the differences in the maps of the estimated $PM_{2.5}$ concentration obtained using the two satellites were also explored.

2. Study area and data

2.1. Study area and ground-level $PM_{2.5}$ measurements

The study area was China, and the study period was from April 2018 to March 2019. The hourly $PM_{2.5}$ concentration data for this study area during the study period were obtained from the China National Environmental Monitoring Station based on a cooperation agreement, and approximately 1500 measurement sites were used. The distribution of the $PM_{2.5}$ concentration monitoring stations is shown in Fig. 1. Due to the number and distribution of monitoring stations, the monitoring of the $PM_{2.5}$ concentration sites were relatively uneven. The density of the monitoring stations in Eastern China was greater than that in Western China due to the topography and the level of urbanization. We only used the data from 10:00 to 17:00 local time (LT), and we removed invalid concentrations of greater than 2000 $\mu g/m^3$ and less than 1 $\mu g/m^3$.

2.2. Satellite data

2.2.1. FY-4A

FY-4A is equipped with an advanced geosynchronous radiation imager (AGRI) with 14 spectral bands. Table 1 shows the spectral bands and spatial resolution of the AGRI on board FY-4A. The 14 bands of AGRI are sampled at a nominal 0.5/1 km spatial resolution at a nadir in the visible bands, 2 km in the near-infrared bands, and 4 km in the infrared bands. As the AOD can be retrieved via an atmospheric radiative transfer model in which the TOA reflectance at three wavelengths (0.620–0.670 μm, 0.459–0.479 μm, and 2.105–2.155 μm) and observation angles (satellite zenith angle, SAZ; satellite azimuth angle, SAA; solar zenith angle, SOZ; and solar azimuth angle, SOA) are utilized as model inputs (Kaufman et al., 1997; Hsu et al., 2004), the TOA reflectance and four observation angles were extracted in this study.

Table 1
Comparison of the bands for FY-4A/AGRI and Himawari-8/AHI.

Channel	FY-4A/AGRI		Himawari-8/AHI	
	Wavelength (μm)	Spatial resolution (km)	Wavelength (μm)	Spatial resolution (km)
Visible bands	0.45–0.49	1	0.43–0.48	1
	-		0.50–0.52	1
	0.55–0.75	0.5–1	0.63–0.66	0.5
	0.75–0.90	1	0.85–0.87	1
Short-wave infrared bands	1.36–1.39	2	-	-
	1.58–1.64	2	1.60–1.62	2
	2.1–2.35	2–4	2.25–2.27	2
Mid-wave infrared bands	3.5–4.0 (High)	2	3.74–3.96	2
	3.5–4.0 (Low)	4	-	-
Water vapor bands	5.8–6.7	4	6.06–6.43	2
	-	-	6.89–7.01	2
	6.9–7.3	4	7.26–7.43	2
Thermal infrared bands	8.0–9.0	4	8.44–8.76	2
	-	-	9.54–9.72	
	-	-	10.3–10.6	
	10.3–11.3	4	11.1–11.3	2
	11.5–12.5	4	12.2–12.5	2
	13.2–13.8	4	13.2–13.4	2

The yellow shading indicates the reflectance data used in this study.

“High” represents the high temperature channel, the monitoring targets are fire points, and the surfaces with strong solar reflections during the day.

“Low” represents the low temperature channel, which is mainly used for low cloud and fog monitoring.

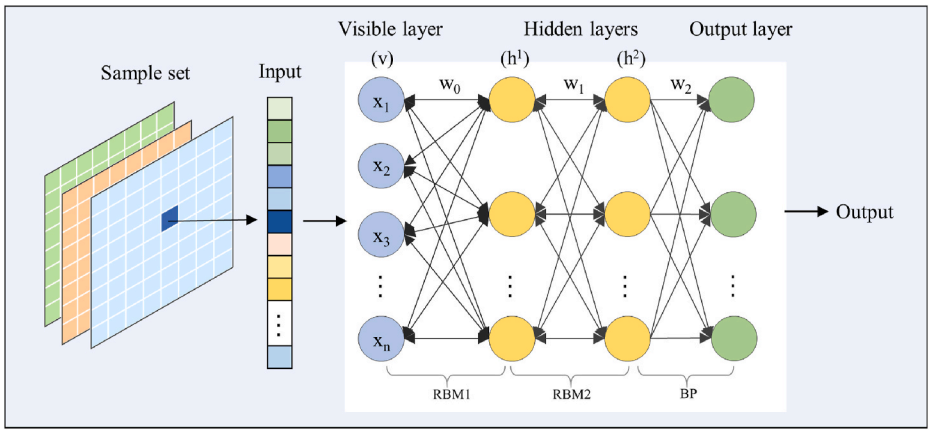

Fig. 2. The structure of the DBN model.

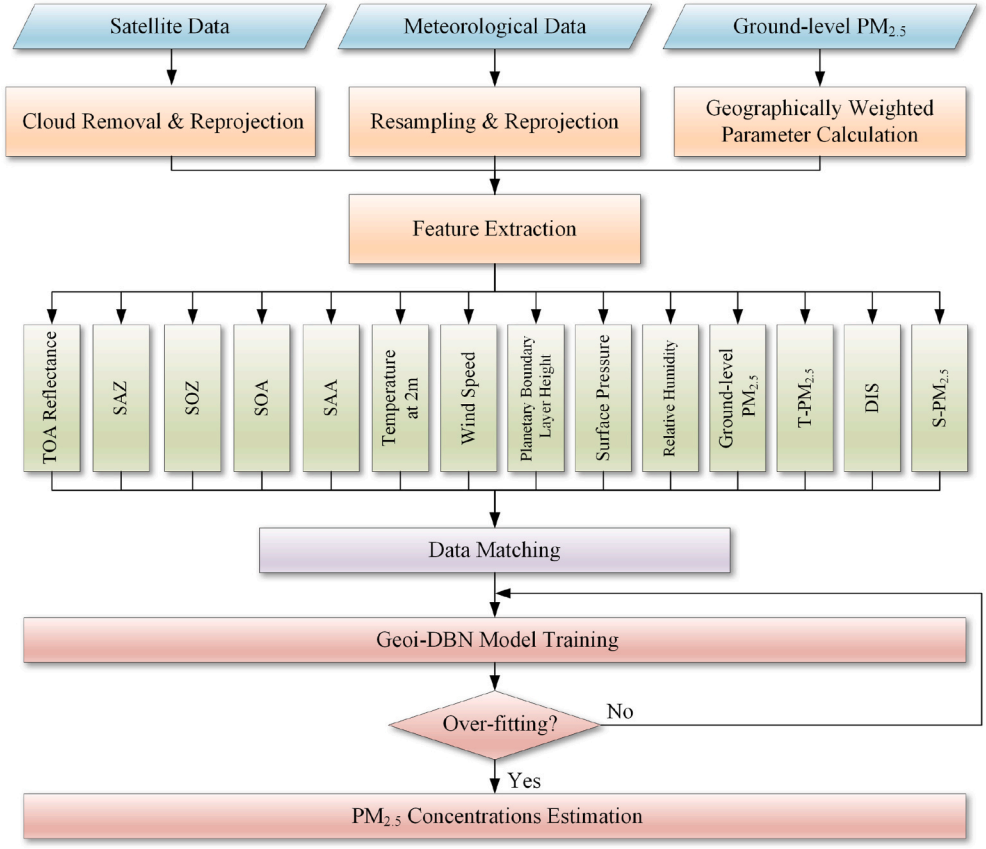

Fig. 3. Experiment flowchart.

In this study, the data collected by the FY-4A satellite were obtained from the National Meteorological Center (http://satellite.nsmc.org.cn), and the reflectance products with a spatial resolution of 4 km were selected. The TOA reflectance data for two bands (0.45–0.49 and 2.1–2.35 μm) were acquired for this study due to the setting of the satellite bands. The 0.55–0.75 μm band data were not used because this band of the FY-4A was wider than that of MODIS (0.62–0.67 μm), including part of the green light band, which is not conducive to AOD retrieval. To eliminate the influence of clouds, the FY-4A cloud mask products with a resolution of 4 km were employed. The cloud mask products have four confidence levels: cloudy, probably cloudy, probably clear, and clear. In this study, only the highest confidence level data (clear) was used.

2.2.2. *Himawari-8*

Himawari-8 is the world's first stationary meteorological satellite that can acquire color images. The frequency of Himawari-8 observations has been increased to once every 10 min to continuously observe cloud and storm movements (Okuyama et al., 2015). The satellite has a design life of more than 15 years and is used to monitor disaster prevention fields, such as storm clouds, typhoon trends, and continuously erupting volcanoes. Table 1 shows the spectral bands and spatial resolution of the AHI on board Himawari-8.

For better comparison with the FY-4A data, we used the 5 km, Level 1B, full-disk calibrated reflectance products obtained from the Japan Aerospace Exploration Agency P-Tree system (ftp://ftp.ptree.jaxa.jp/). We selected band 1, band 6, and four observation angles (SAZ, SAA,

SOZ, and SOA) as part of the input data. Due to the limited observation range of 80–200°E and 60°S–60°N and considering the data quality problems in the marginal areas, the SAZ data for >68° were eliminated to avoid a low estimation accuracy. The level 2 Cloud products were utilized to remove the cloud-contaminated TOA reflectance.

2.3. Meteorological parameters

The Goddard Earth Observing System Data Assimilation System GEOS-5 Forward Processing (GEOS 5-FP) meteorological data were used in this study. These GEOS 5-FP meteorological data have a spatial resolution of 0.25° latitude × 0.3125° longitude. Meteorological factors, including the temperature at 2 m (TEMP, K), the wind speed components at 10 m (WS, m/s), the planetary boundary layer height (PBLH, m), surface pressure (PS, kPa), and relative humidity (RH, %), were also used as predictors to support the $PM_{2.5}$ concentration mapping. To facilitate the subsequent modeling, all of the meteorological data were resampled to spatial resolutions of 4 and 5 km using the bilinear interpolation method.

3. Model and validation

3.1. The Geoi-DBN model

The $PM_{2.5}$ concentration is affected by many factors, among which complex nonlinear relationships exist. Deep learning is a very effective mean of determining the relationships between complex variables. In this study, we used the Deep Belief Net (DBN) model, which is one of the most typical deep learning models, to predict the spatial and temporal distributions of the $PM_{2.5}$ concentration (Hinton et al., 2006). It is composed of multiple restricted Boltzmann machine (RBM) layers and a back-propagation (BP) layer (Fig. 2). An RBM is composed of a visible layer (v) and a hidden layer (h), both of which are connected by weights (W), and the hidden layer of the previous RBM is the visible layer of the next RBM. We chose two RBM layers and one BP layer as our prediction model and defined the $PM_{2.5}$ concentration as a response variable and the others as predictors in the DBN model. The structure is as follows:

$$PM_{2.5} = f(TOA, Angles, Wea, S-PM_{2.5}, T-PM_{2.5}, DIS) \quad (1)$$

where *Angles* denotes the observation angles, including the SAZ, SAA, SOZ, and SOA; and *Wea* denotes the TEMP, WS, PBLH, PS, and RH. $S-PM_{2.5}$ $T-PM_{2.5}$, and *DIS* are collectively referred to as the geographical correlation of the $PM_{2.5}$ concentration (Li et al., 2017a). S-$PM_{2.5}$ and T-$PM_{2.5}$ consider the spatial and temporal autocorrelations of the $PM_{2.5}$ concentration, and DIS is incorporated to reflect the spatial heterogeneity of the unevenly distributed stations. These three parameters are calculated by the nearby n grids of the $PM_{2.5}$ concentration measurements and the $PM_{2.5}$ concentration observation from the m prior days for the same grid, which can be expressed as follows:

$$S-PM_{2.5} = \frac{\sum_{i=1}^{n} ws_i PM_{2.5,i}}{\sum_{i=1}^{n} ws_i} \quad ws_i = \frac{1}{ds_i^2} \quad (2)$$

$$T-PM_{2.5} = \frac{\sum_{j=1}^{m} wt_j PM_{2.5,j}}{\sum_{j=1}^{m} wt_j} \quad wt_j = \frac{1}{dt_j^2} \quad (3)$$

$$DIS = \frac{1}{\min(ds_i)} \quad i = 1, 2, \ldots, n \quad (4)$$

where *ds* and*dt* refer to the spatial and temporal distances, respectively. In addition, we set n = 30 and m = 3 to ensure the computational efficiency while guaranteeing the predictive accuracy.

Fig. 3 shows the data pre-processing and modeling processes. First, all of the data were collected, resampled, and converted into the same coordinate system. Then, the grids of the multiple variables were matched on a specific hourly scale. A multivariate vector was obtained for each labeled grid, which is the form of the model input sample. Second, this multi-dimensional vector was input into the DBN model. During the modeling, the model extracted the basic features associated with the $PM_{2.5}$ concentration and transferred them from the previous RBM to the next RBM layer. The initial weights of the DBN were generated through pre-training of the RBM. Then, we were able to calculate the estimated error between the estimated $PM_{2.5}$ concentration and the ground-based $PM_{2.5}$ measurement. The estimation error was sent back to the BP layer until the error reached a satisfactory level. Finally, to evaluate whether the model experienced over-fitting, 10-fold cross validation was performed on the model. The details are presented in Section 3.2.

3.2. Model validation

For the 10-fold cross validation, the entire training dataset was randomly and averagely divided into 10 subsets, and nine of the subsets were used for the model training. The remaining dataset was used for the model validation. The abovementioned process was repeated until each subset had been used for the model validation. In this study, three 10-fold cross-validation (CV) methods were used to test the independence of the training data: the sample-based CV, site-based CV, and a CV-based validation approach, which considers the uneven spatial distribution of the monitoring stations (denoted as SDCV) (Li et al., 2020).

The sample-based CV is the most commonly used CV-based validation approach. Thus, the sample-based CV involves conducting the validation with integrated samples from both the spatial and temporal dimensions, and it is often employed to reflect the overall predictive ability of $PM_{2.5}$ estimation models. For a certain monitoring station, the samples at a certain time for this station can be used for the model fitting, while the samples at the other times are used for the model validation. Consequently, the sample-based CV has limitations, which introduces some bias when assessing the predictive ability of a model.

Different from the sample-based CV, the site-based CV randomly selects monitoring sites for the model validation. For the site-based CV, the validation sites are never involved in the model fitting, and thus, it can suitably reflect the spatial prediction capability of the model. In addition, the monitoring sites are often located in central urban areas, so the validation sites are very close to the modeling sites. Therefore, the site-based CV generally only reflects the model's performance at locations closer to the monitoring sites, and it cannot assess the estimation accuracy at locations farther away from the monitoring sites.

To more comprehensively and effectively evaluate and the prediction model, Li et al. (2020) proposed the SDCV, which considers the uneven spatial distribution of the monitoring stations. The SDCV introduces the spatial distance between the validation station and the modeling station into the CV process, and it evaluates the spatial performance by excluding modeling stations within a specific distance. The SDCV can yield a more effective evaluation of the popular $PM_{2.5}$ estimation models than the traditional validation approaches. This method requires setting a distance (d) and removing the modeling stations with a distance to any validation station of less than d. It can reflect the estimated accuracy of the region far away from the monitoring sites better. In this study, we set d = 90 km as the optimal distance in China. The coefficient of determination (R^2), the root-mean-square error (RMSE, $\mu g/m^3$), the mean prediction error (MPE, $\mu g/m^3$), and the relative prediction error (RPE, %) were used for the quantitative evaluation. The closer R^2 is to 1, the stronger the estimation ability is. The smaller the RMSE, MPE, and RPE values are, the better the model is.

Table 2
The cross-validation performances of FY-4A (4 km) and Himawari-8 (5 km).

Data	Sample-based CV				Site-based CV				SDCV			
	R^2	RMSE	MPE	RPE	R^2	RMSE	MPE	RPE	R^2	RMSE	MPE	RPE
FY-4A (914380)	0.93	8.18	4.97	0.23	0.84	12.61	7.59	0.35	0.53	21.80	13.46	0.61
Himawari-8 (838818)	0.93	9.49	5.60	0.24	0.86	13.59	8.00	0.34	0.57	24.22	14.83	0.61

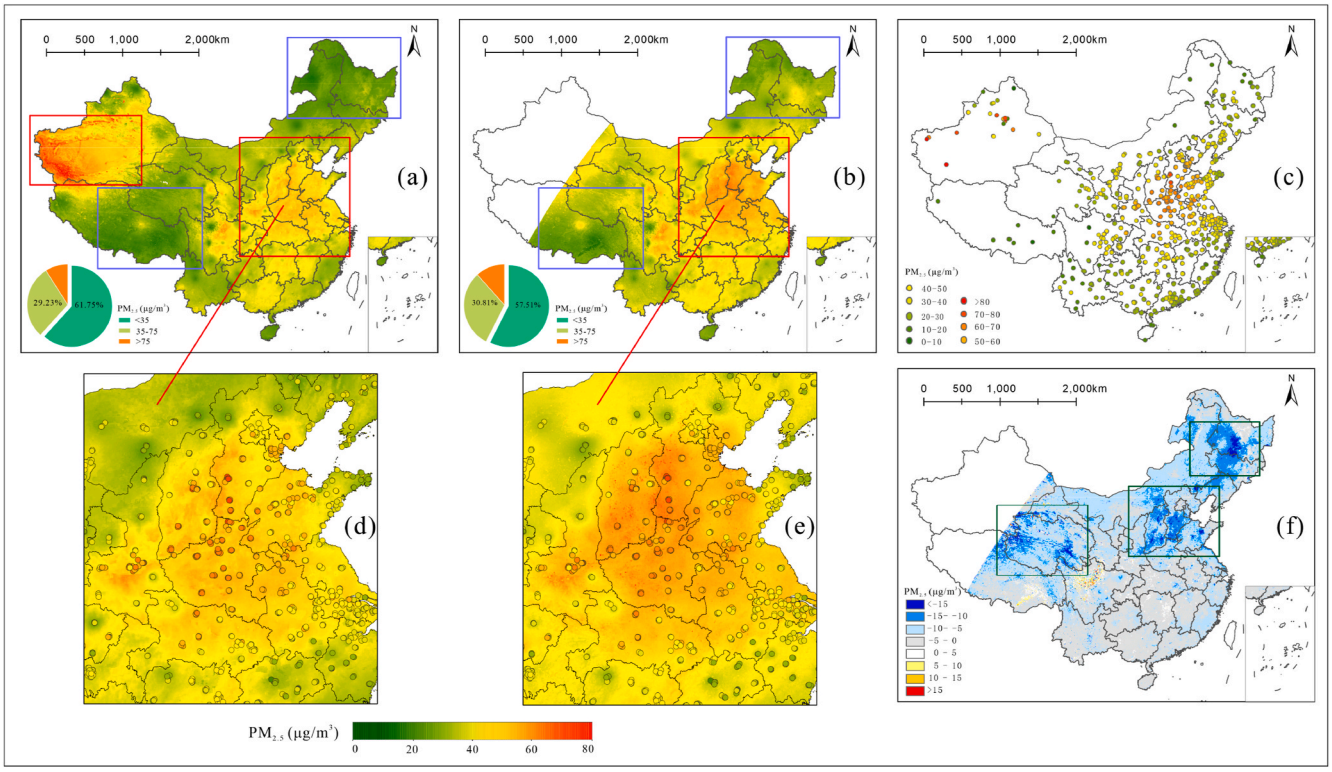

Fig. 4. Yearly average $PM_{2.5}$ concentration estimation results obtained using the (a) FY-4A and (b) Himawari-8 data and (c) ground-level measured $PM_{2.5}$ concentrations in China. (d) and (e) show the details of the areas enclosed by the red frame. The points indicate $PM_{2.5}$ concentrations measured by the monitoring stations. (f) shows the difference between the annual average results of FY-4A and the average annual results of Himawari-8. The pie charts in (a) and (b) show the distributions of the $PM_{2.5}$ concentrations of the training data. (For interpretation of the references to color in this figure legend, the reader is referred to the Web version of this article.)

4. Results and discussion

4.1. Overall evaluation

The sample size of the FY-4A modeling dataset (N = 914380) was slightly larger than that of the Himawari-8 modeling dataset (N = 838818) due to their different spatial resolutions and cloud mask products. From the perspective of the quantitative evaluation presented on Table 2, by using the sample-based CV to evaluate the DBN model, FY-4A was found to have the superior performance (R^2 of 0.93 and RMSE of 8.18). The R^2 values of FY-4A and Himawari-8 were the same, but the RMSE, MPE, and RPE values of FY-4A were smaller than those of Himawari-8. For the site-based CV, the R^2 value was 0.84 for FY-4A, which was lower than that of the Himawari-8 model (0.86). The RMSE and MPE for FY-4A were 12.61 and 7.59 μg/m^3, respectively, which were lower than those for Himawari-8 (13.59 and 8.00 μg/m^3, respectively). In addition, for the SDCV, the R^2 of FY-4A was lower than that of Himawari-8, and the RMSE and RPE of FY-4A were lower than those of Himawari-8. The evaluation results of the site-based and SDCV validations were similar. The results indicate that FY-4Y performed better in terms of the overall prediction ability of the $PM_{2.5}$ estimation model, but from the perspective of the spatial prediction ability, the Himawari-8 model had a superior predictive power. In addition, it should be noted that the $PM_{2.5}$ concentration retrieved from the Himawari-8 data was more consistent with the trend of the ground $PM_{2.5}$ concentration, but the error evaluation indexes (RMSE, MPE, and RPE) were slightly larger than those of FY-4A based on the results of the two spatial CV methods. One reason for this is that Himawari-8 cannot cover the western region of China due to the limitation of its observation range. Therefore, the coverage of the two satellite-based training samples was inconsistent. The lack of ground stations in the western region resulted in too few sample points, so the model had difficultly fully explaining the relationship between the $PM_{2.5}$ concentration and the influencing factors, and the accuracy of the $PM_{2.5}$ estimation was significantly lower in the western region than the region with more stations. This means that the higher R^2 values of Himawari-8 for both validation methods could be due to inconsistent data.

Fig. 4 shows the annual mean distributions of the estimated $PM_{2.5}$ concentrations obtained using the FY-4A satellite data and the Himawari-8 satellite data and the ground-level measured $PM_{2.5}$ concentrations in China. The different scanning ranges of FY-4A and Himawari-8 led to a lack of observation data in most parts of Xinjiang and Tibet. High-value regions were observed in the inland regions (the Beijing-Tianjin-Hebei region, Shanxi, Henan, Anhui, Shandong, Jiangsu, Shanxi, and Hubei provinces), which are enclosed by the red frame. In contrast, low-value areas were observed in the regions enclosed by the

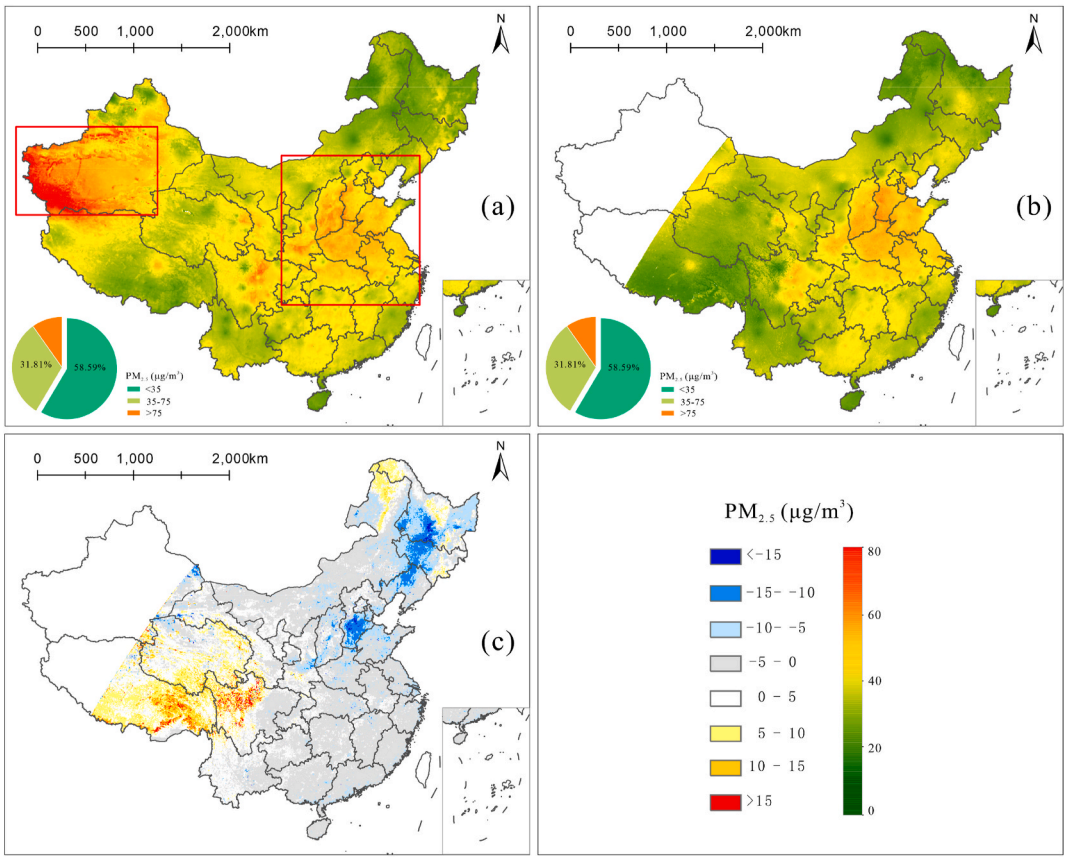

Fig. 5. Yearly average $PM_{2.5}$ concentration estimation results for a 5-km resolution using the (a) FY-4A and (b) Himawari-8 data; and (c) difference between the annual average result of FY-4A and the average annual result of Himawari-8 for a 5-km resolution. The pie charts in (a) and (b) represent the distributions of the $PM_{2.5}$ concentration in the training data.

Table 3
The cross-validation performances of FY-4A (5 km) and Himawari-8 (5 km).

Data	Sample-based CV				Site-based CV				SDCV			
	R^2	RMSE	MPE	RPE	R^2	RMSE	MPE	RPE	R^2	RMSE	MPE	RPE
FY-4A (633442)	0.93	8.25	5.10	0.22	0.85	12.22	7.65	0.33	0.53	21.60	13.95	0.57
Himawari-8 (633442)	0.93	8.27	5.12	0.22	0.85	12.12	7.58	0.32	0.52	21.54	14.10	0.57

Table 4
The cross-validation performances of FY-4A and Himawari-8 with the original spatial resolution.

Data	Sample-based CV				Site-based CV				SDCV			
	R^2	RMSE	MPE	RPE	R^2	RMSE	MPE	RPE	R^2	RMSE	MPE	RPE
FY-4A (4KM)	0.93	8.22	5.10	0.23	0.85	12.19	7.69	0.33	0.52	21.71	14.01	0.58
Himawari-8 (5KM)	0.93	8.27	5.12	0.22	0.85	12.12	7.58	0.32	0.52	21.54	14.10	0.57

blue frame. The high $PM_{2.5}$ values were mainly due to intensive human activities, industrial factories, and frequent dust events. In addition, the details of the $PM_{2.5}$ concentration compared with the ground station values are shown in Fig. 4(d) and (e). For the high-value regions, the yearly average estimated concentrations of FY-4A and Himawari-8 were 42.77 μg/m^3 and 49.17 μg/m^3, respectively. The yearly average concentration of the ground stations was 49.54 μg/m^3, and thus, FY-4A provided an obvious underestimation, while Himawari-8 provided results close to the values measured by the monitoring stations. A high level of $PM_{2.5}$ pollution was found in the northern part of Xinjiang due to the effect of dust particles from the desert region. To further discuss the differences in the distribution of the $PM_{2.5}$ concentration estimated using data from the two satellites, Fig. 4(f) presents the differences between the two mapping results (Fig. 4 (a) and (b)). Most of the areas were in the range of −5–0 μg/m^3, and large errors of less than −15 μg/m^3 occurred in the area surrounded by the dark green box in Fig. 4(f). Most of the areas in China showed higher estimated $PM_{2.5}$ concentrations based on the Himwari-8 data than based on the FY-4A data.

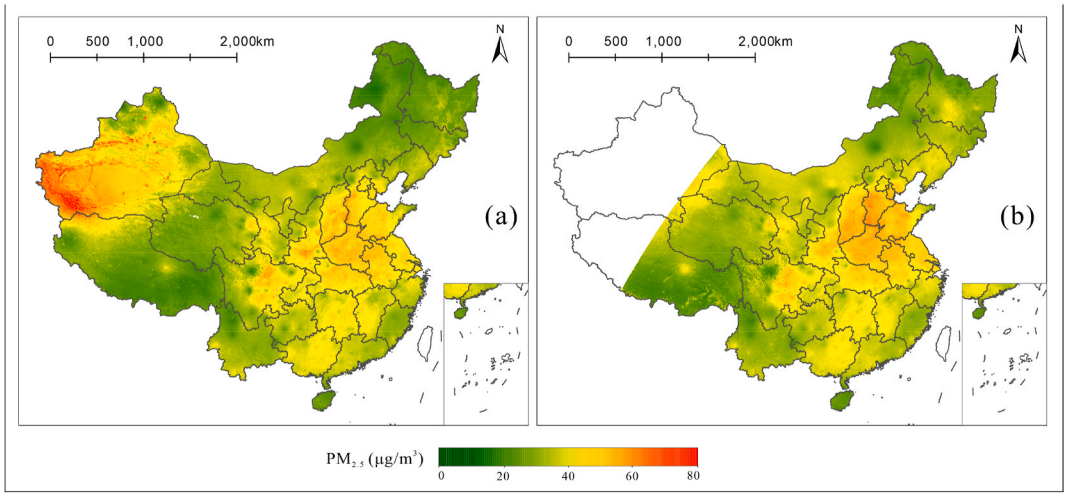

Fig. 6. Yearly average $PM_{2.5}$ estimation results obtained using the (a) FY-4A (4 km) and (b) Himawari-8 (5 km) common data.

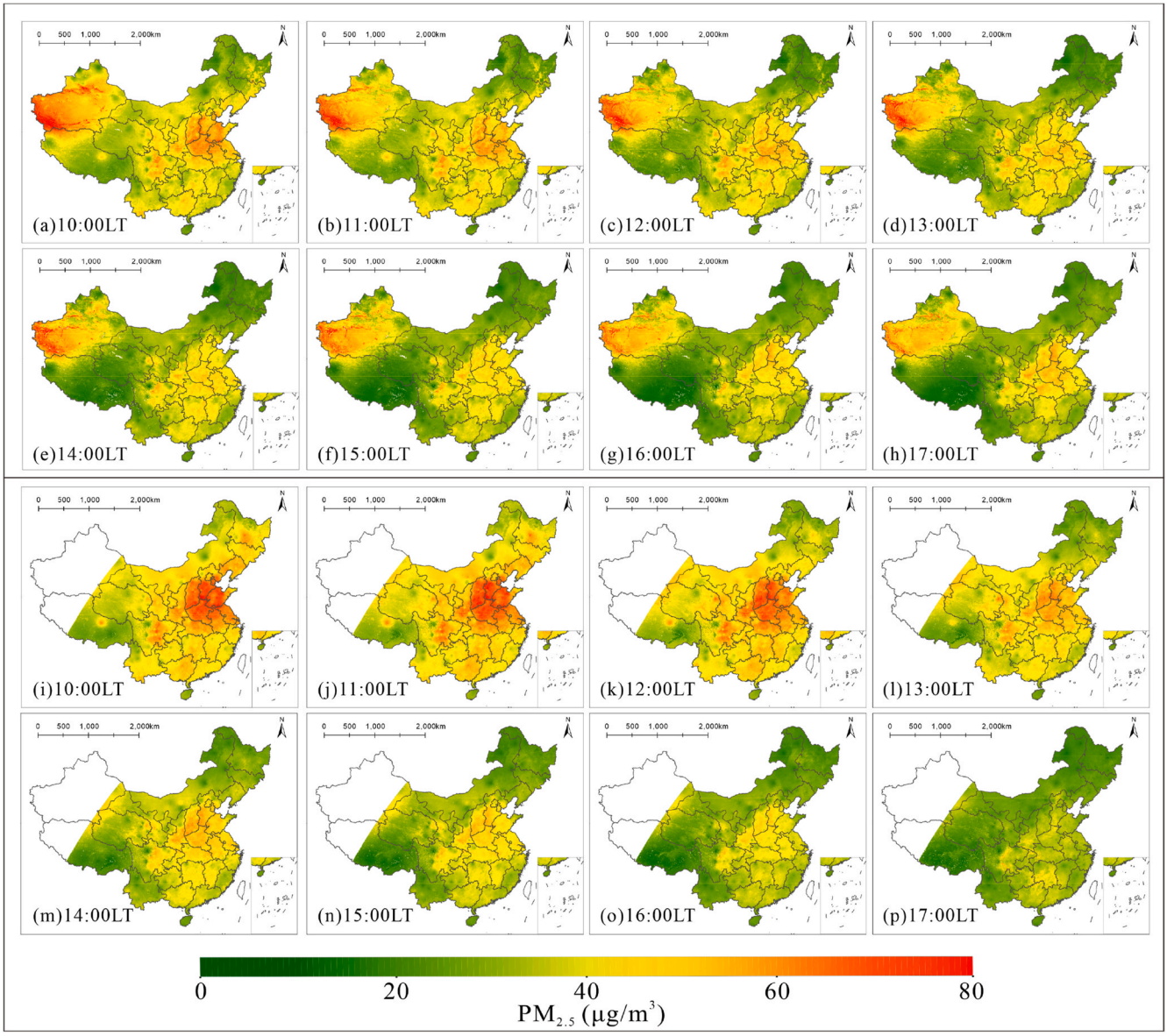

Fig. 7. Hourly distribution of the estimated $PM_{2.5}$ concentration.

Table 5
The proportion of high (>35 μg/m^3) and low (≤35 μg/m^3) values for each hourly training dataset.

Time	FY-4A		Himawari-8	
	High (%)	Low (%)	High (%)	Low (%)
10:00LT	46.98	53.02	52.80	47.20
11:00LT	43.67	56.33	50.09	49.91
12:00LT	39.89	60.11	45.61	54.39
13:00LT	36.63	63.37	41.45	58.55
14:00LT	33.74	66.26	37.83	62.17
15:00LT	31.63	68.37	34.95	65.05
16:00LT	31.36	68.64	30.84	69.16
17:00LT	31.67	68.33	23.21	76.79

Taking these phenomena into consideration, we tentatively identified the main reasons for the differences in the estimations.

1) Difference in spatial resolution. The resolution of FY-4A was 4 km, whereas that of Himawari-8 was 5 km, resulting in different levels of mapping details.
2) Differences of training sets. The differences in the training sets can be divided into number differences and regional differences. The number differences were caused by the different cloud masks, and the regional differences were caused by the coverages of the satellite platforms.
3) Differences in the platforms and the retrieval algorithms. The platform differences include the observation angles, imaging quality, and platform movement. The influence of the retrieval algorithm was reflected in the training process, and the model was built using the TOA data and the ground $PM_{2.5}$ concentrations. The influence of the platform variability that was eliminated using the model training was difficult to assess, so we considered them as one influencing factor here.

To explore which factors affected the mapping results, we thoroughly investigated the causes (see Sections 4.2 and 4.3).

4.2. Influence of the differences in the satellite platforms and retrieval algorithms

To further determine which of the two satellites is more advantageous, the influences of the satellites' platforms and retrieval algorithms were investigated. The common monitoring stations used for the FY-4A and Himawari-8 data training were selected, and the FY-4A satellite data were resampled to 5 km. The number of the new common datasets was 633442, and the common datasets were input into the models for training. The distributions of the estimated $PM_{2.5}$ concentrations with a 5-km resolution are shown in Fig. 5. The differences between the two results are not significant. Compared with Fig. 4, the overall concentration from FY-4A increased. The $PM_{2.5}$ concentration values in the red frame are higher than those in Fig. 4(a) and are close to the results from Himawari-8. The yearly average estimated $PM_{2.5}$ concentration of FY-4A was 38.65 μg/m^3, which is 6 μg/m^3 higher than the previous result. The yearly estimated $PM_{2.5}$ concentration of Himawari-8 was 32.00 μg/m^3, which is not much smaller than the previous result (35.64 μg/m^3). In addition, we also estimated the yearly average $PM_{2.5}$ result of FY-4A minus the result of Himawari-8, and the difference is shown in Fig. 5 (c). Compared with Fig. 4(f), obvious positive number regions occur in southwestern and northeastern China, demonstrating that the annual average estimated values of FY-4A in these areas were higher than the annual average estimated values of Himawari-8. The area in the range of −10 to −5 μg/m^3 was smaller than that in Fig. 4(f), and most of the regions were in the area of −5–0 μg/m^3. In northeastern China and northern China, they were still <−10 μg/m^3, but the coverage area and the value of the differences decreased. The estimated values of Himawari-8 were lower than before, but they were still higher than those of FY-4A.

To further analyze the differences between Figs. 4 and 5, the percentage of the ground $PM_{2.5}$ concentration participating in the model training was calculated. The results are shown in Figs. 4 and 5. Among the training sample sets for FY-4A (Fig. 4(a)), the low values accounted for a large proportion (61.75%), and the percentage of low values for Himawari-8 in the training (Fig. 4(b)) was lower, reaching 57.51%. In this experiment, the low value of the common sample set (Fig. 5(a)) was 58.59%. For the FY-4A training data, the proportion of low values decreased, and the proportion of high values participating in the training increased. Thus, the common mapping result showed an increasing trend in the $PM_{2.5}$ concentration compared to Fig. 4(a). For the Himawari-8 training data, the proportion of low values did not change much. Compared to the proportion of low values in the Himwari-8 training set described in Section 4.1, the proportion of low values only increased by 1.08%. Therefore, there was a slight reduction in the mapping result of the Himawari-8 based on the common dataset.

The evaluation results of the experiment are shown in Table 3. For the sample-based CV and the site-based CV, the R^2 values of FY-4A (0.93 and 0.85, respectively) were the same as those of Himawari-8 (0.93 and 0.85, respectively); while the RMSE values for FY-4A were 8.25 and 12.22, respectively, and those of Himawari-8 were 8.27 and 12.12 μg/m^3, respectively. For FY-4A and Himawari-8, the SDCV R^2 values were 0.53 and 0.52, respectively; the RMSE values were 21.60 and 21.54 μg/m^3, respectively; the MPE values were 13.95 and 14.10 μg/m^3, respectively; and the RPE values were 0.57 and 0.57, respectively. From the point of view of the quantitative indicators, the results obtained using the two satellites were similar, but FY-4A exhibited a resampling error. According to the resampling evaluation experiment, the performance of the Geoi-DBN model was not sensitive to the resampling error (Table S). Exclude the resampling error, the accuracy evaluation and mapping of FY-4A were not significantly different from those of Himawari-8. Thus, we conclude that the estimated differences were caused by the differences in the training data and the spatial resolution, excluding the differences in the platforms and retrieval algorithms.

4.3. Influence of the differences in spatial resolutions

According to the analysis presented in Section 4.2, the current difference was caused by the spatial resolution or the number and the

Table 6
Hourly averaged $PM_{2.5}$ concentration estimation results obtained using FY-4A and Himawari-8.

Data	FY-4A					Himawari-8				
Time	N	R^2	RMSE	MPE	RPE	N	R^2	RMSE	MPE	RPE
10:00LT	134059	0.93	9.19	5.77	0.22	125465	0.93	10.76	6.49	0.23
11:00LT	112690	0.92	9.02	5.66	0.23	120552	0.92	11.32	6.71	0.24
12:00LT	97340	0.92	8.50	5.36	0.23	114797	0.93	10.31	6.26	0.24
13:00LT	84707	0.91	8.45	5.17	0.24	110362	0.93	9.52	5.81	0.24
14:00LT	95837	0.92	7.72	4.73	0.23	111022	0.94	8.92	5.29	0.24
15:00LT	114153	0.93	7.71	4.62	0.24	104744	0.94	8.27	4.88	0.23
16:00LT	132324	0.94	7.83	4.59	0.23	93197	0.94	7.41	4.40	0.23
17:00LT	143270	0.95	7.50	4.38	0.22	58679	0.91	5.94	3.67	0.22

region of the training dataset. Therefore, we selected the common regionally ground-based stations used for the FY-4A and Himawari-8 data training based on the original spatial resolution.

For the sample-based CV (Table 4), the R^2 and RMSE values of FY-4A were 0.93 and 8.22 μg/m^3, respectively, and those of Himawari-8 were 0.93 and 8.27 μg/m^3, respectively. For the site-based CV, values of the four evaluation indicators (R^2, RMSE, MPE, and RPE) were similar, but the FY-4A results had slightly larger errors. A similar situation was found for the results of the SDCV. Based on the quantitative evaluation results, it was not obvious which satellite data had a higher accuracy. By comparing the mapping results presented in Fig. 6, the mapping results of FY-4A were found to be similar to the original results (Fig. 4(a)), but they are still different from the high value area of Himawari-8. Thus, the differences in the mapping were due to the spatial resolution and the number of training sets caused by the different spatial resolutions, excluding the influence of the training set regional differences.

4.4. Mapping the hourly spatiotemporal distribution of $PM_{2.5}$

To further compare the temporal changes in the $PM_{2.5}$ concentration obtained from the two satellites, the hourly $PM_{2.5}$ concentration data were modeled. The results of the hourly mapping are shown in Fig. 7. For the mapping based on the FY-4A data, the $PM_{2.5}$ concentration was generally high at 10:00 LT. As time progressed, the $PM_{2.5}$ pollution was alleviated from 11:00 LT to 15:00 LT. Later, the $PM_{2.5}$ concentration started to increase again at 16:00 LT due to the increased traffic at the end of the work day. In addition, from 10:00 LT to 17:00 LT, the $PM_{2.5}$ concentration slightly changed in the western part of Xinjiang Province. The mapping result for Himawari-8 is similar to the above trends, but the $PM_{2.5}$concentration did not increase at 17:00 LT because more data were missing at 16:00 LT (N = 93197) and 17:00 LT (N = 58679). There were some differences in the hourly details of the FY-4A and the Himawari-8 mappings. For example, the $PM_{2.5}$ concentrations in central China were higher for Himwari-8 than FY-4A, especially in the Beijing-Tianjin-Hebei region and Shanxi, Henan, and Shandong provinces. The mean $PM_{2.5}$ concentration for Himawari-8 in the above provinces at 10:00 LT was 64.43 μg/m^3, which was approximately 12 μg/m^3 higher than the average concentration for FY-4A. From 10:00 LT to 12:00 LT, the rate of decrease of the $PM_{2.5}$ concentration was slower than that for FY-4A. This occurred because the hourly mapping results were obtained by training all of the samples, and based on the analysis of the $PM_{2.5}$ concentration distribution of the sample data presented in Section 4.1, the proportion of low values for FY-4A was higher and the proportion of high values was lower compared with those for Himawari-8. Thus, the performances of the model in terms of fitting the high and low values were different for the Himawari-8 and FY-4A satellite datasets. Based on this, Table 5 summarizes the statistical results of the proportions of high and low values for each hourly training dataset. Here, the high and low values were set according to the environmental control quality standards in China. The $PM_{2.5}$ index was less than 35 μg/m^3, which is considered to be an excellent air quality level. On a given day, from 10:00 LT to 15:00 LT, the proportion of high values was higher for Himawari-8 than for FY-4A, and the magnitude of the differences decreased with time. After 16:00 LT, the percentage of high values for FY-4A gradually became higher than that for Himawari-8. This could explain why the $PM_{2.5}$ concentration of Himwari-8 was higher at the beginning of the day, but lower than that of FY-4A at 17:00 LT.

Table 6 shows the evaluation results of the accuracy of the hourly averaged $PM_{2.5}$ concentration estimation (from 10:00 LT to 17:00 LT). The R^2 values were all higher than 0.91 for FY-4A and Himawari-8, and the maximum value was 0.95, which suggests that the model was relatively stable in each hour and had a high performance. Except for 17:00 LT, the RMSE values of Himawari-8 for each hour were higher than those of FY-4A. The most data FY-4A were missing at 13:00, and the R^2 value was the lowest. The most Himawari-8 data were missing at 17:00, and its R^2 value was also the lowest, thereby indicating that the amount of data affected the R^2. At 17:00 LT, 58679 samples were found, and this number was lower than the 10:00 LT samples by more than half. The Himawari-8 satellite's observation position made it difficult to obtain high-quality data at 17:00 LT in China.

In general, geostationary satellites with high temporal resolutions need to be used so that we can identify the dynamic changes in the $PM_{2.5}$ contribution and contribute to environmental monitoring and health impact assessment.

5. Conclusions

Using geostationary satellites to estimate the continuously distributed $PM_{2.5}$ concentration is significant for environmental governance and health risk research. In this study, FY-4A and Himawari-8 TOA reflectance data combined with auxiliary data were used as the model training datasets. The Geoi-DBN model was introduced to investigate the complex relationships among the input datasets. The conclusions of this study are as follows.

1) By comparing the quantitative evaluation and mapping results of FY-4A and Himawari-8, FY-4A was found to be more suitable for predicting the $PM_{2.5}$ concentration in China than Himawari-8 because FY-4A has a more comprehensive spatial coverage and higher accuracy.
2) The mapping differences between the $PM_{2.5}$ concentrations estimated using FY-4A and Himawari-8 data were due to the differences in their platforms, retrieval algorithms, and spatial resolutions and the training datasets used for the model. Among them, the platform and retrieval algorithms had the least influence.
3) The predictive performances of the Geoi-DBN were robust during the day-time hours, and the R^2 values were all >0.9, but differences were observed. These differences were related to the sizes of the training datasets.

This study is of great significance for improving the use of geostationary satellites in atmospheric environment remote sensing research. The Fengyun-4B satellite was successfully launched from Xichang City on June 3, 2021. Its successful launch marked the official beginning of the operational development stage of China's new generation of geostationary orbit satellite observation systems. Thus, future work should focus on using domestic satellite data to monitor $PM_{2.5}$ concentrations in real time.

CRediT authorship contribution statement

Yuqing Hu: Data curation, Methodology, Validation, Software, Formal analysis, Writing – original draft. **Chao Zeng:** Project administration, Formal analysis, Writing – review & editing, Supervision. **Tongwen Li:** Methodology, Writing – review & editing, Supervision. **Huanfeng Shen:** Investigation, Supervision.

Declaration of competing interest

The authors declare that they have no known competing financial interests or personal relationships that could have appeared to influence the work reported in this paper.

Acknowledgements

This research was funded by Special Technology Innovation Major Project of Hubei Province, China (2019AAA046) and the National Key R&D Program of China (No.2019YFB2102900). The authors are also grateful to the National Satellite Meteorological Center (NSMC), Japan Aerospace Exploration Agency (JAXA) and the Goddard Space Flight Center Distributed Active Archive Center (GSFC DAAC) for supporting the data.

Appendix A. Supplementary data

Supplementary data to this article can be found online at https://doi.org/10.1016/j.atmosenv.2021.118898.

References

Bartell, S.M., Longhurst, J., Tjoa, T., Sioutas, C., Delfino, R.J., 2013. Particulate air pollution, ambulatory heart rate variability, and cardiac arrhythmia in retirement community residents with coronary artery disease. Environ. Health Perspect. 121, 1135–1141. https://doi.org/10.1289/ehp.1205914.

Brauer, M., Amann, M., Burnett, R.T., Cohen, A., Dentener, F., Ezzati, M., Henderson, S. B., Krzyzanowski, M., Martin, R.V., Van Dingenen, R., van Donkelaar, A., Thurston, G.D., 2012. Exposure assessment for estimation of the global burden of disease attributable to outdoor air pollution. Environ. Sci. Technol. 46, 652–660. https://doi.org/10.1021/es2025752.

Cohen, A.J., Brauer, M., Burnett, R., Anderson, H.R., Frostad, J., Estep, K., Balakrishnan, K., Brunekreef, B., Dandona, L., Dandona, R., Feigin, V., Freedman, G., Hubbell, B., Jobling, A., Kan, H., Knibbs, L., Liu, Y., Martin, R., Morawska, L., Pope, C.A., Shin, H., Straif, K., Shaddick, G., Thomas, M., van Dingenen, R., van Donkelaar, A., Vos, T., Murray, C.J.L., Forouzanfar, M.H., 2017. Estimates and 25-year trends of the global burden of disease attributable to ambient air pollution: an analysis of data from the Global Burden of Diseases Study 2015. Lancet 389, 1907–1918. https://doi.org/10.1016/S0140-6736(17)30505-6.

Fang, X., Zou, B., Liu, X., Sternberg, T., Zhai, L., 2016. Satellite-based ground $PM_{2.5}$ estimation using timely structure adaptive modeling. Remote Sens. Environ. 186, 152–163. https://doi.org/10.1016/j.rse.2016.08.027.

Guo, B., Zhang, D.M., Pei, L., Su, Y., Wang, X.X., Bian, Y., Zhang, D.H., Yao, W.Q., Zhou, Z.X., Guo, L.Y., 2021. Estimating $PM_{2.5}$ concentrations via random forest method using satellite, auxiliary, and ground-level station dataset at multiple temporal scales across China in 2017. Sci. Total Environ. 778 https://doi.org/10.1016/j.scitotenv.2021.146288.

Guo, H., Cheng, T.H., Gu, X.F., Wang, Y., Chen, H., Bao, F.W., Shi, S.Y., Xu, B.R., Wang, W.N., Zuo, X., Zhang, X.C., Meng, C., 2017. Assessment of $PM_{2.5}$ concentrations and exposure throughout China using ground observations. Sci. Total Environ. 601, 1024–1030. https://doi.org/10.1016/j.scitotenv.2017.05.263.

Gupta, P., Levy, R.C., Mattoo, S., Remer, L.A., Holz, R.E., Heidinger, A.K., 2019. Applying the dark target aerosol algorithm with advanced Himawari imager observations during the KORUS-AQ field campaign. Atmos. Meas. Tech. 12, 6557–6577. https://doi.org/10.5194/amt-12-6557-2019.

Hinton, G.E., Osindero, S., Teh, Y.-W., 2006. A fast learning algorithm for deep belief nets. Neural Comput. 18, 1527–1554. https://doi.org/10.1162/neco.2006.18.7.1527.

Hsu, N.C., Tsay, S.C., King, M.D., Herman, J.R., 2004. Aerosol properties over bright-reflecting source regions. IEEE Trans. Geosci. Rem. Sens. 42, 557–569. https://doi.org/10.1109/tgrs.2004.824067.

Hu, X., Waller, L.A., Lyapustin, A., Wang, Y., Liu, Y., 2014a. 10-year spatial and temporal trends of $PM_{2.5}$ concentrations in the southeastern US estimated using high-resolution satellite data. Atmos. Chem. Phys. 14, 6301–6314. https://doi.org/10.5194/acp-14-6301-2014.

Hu, X.F., Waller, L.A., Lyapustin, A., Wang, Y.J., Al-Hamdan, M.Z., Crosson, W.L., Estes, M.G., Estes, S.M., Quattrochi, D.A., Puttaswamy, S.J., Liu, Y., 2014b. Estimating ground-level $PM_{2.5}$ concentrations in the Southeastern United States using MAIAC AOD retrievals and a two-stage model. Remote Sens. Environ. 140, 220–232. https://doi.org/10.1016/j.rse.2013.08.032.

Kaufman, Y.J., Tanré, D., Remer, L.A., Vermote, E.F., Chu, A., Holben, B.N., 1997. Operational remote sensing of tropospheric aerosol over land from EOS moderate resolution imaging spectroradiometer. J. Geophys. Res. Atmos. 102, 17051–17067. https://doi.org/10.1029/96jd03988.

Kloog, I., Nordio, F., Coull, B.A., Schwartz, J., 2012. Incorporating local land use regression and satellite aerosol optical depth in A hybrid model of spatiotemporal $PM_{2.5}$ exposures in the Mid-Atlantic States. Environ. Sci. Technol. 46, 11913–11921. https://doi.org/10.1021/es302673e.

Koren, I., Dagan, G., Altaratz, O., 2014. From aerosol-limited to invigoration of warm convective clouds. Science 344, 1143–1146. https://doi.org/10.1126/science.1252595.

Lary, D.J., Lary, T., Sattler, B., 2015. Using machine learning to estimate global $PM_{2.5}$ for environmental health studies. Environ. Health Insights 9, 41–52. https://doi.org/10.4137/EHI.S15664.

Levy, R.C., Mattoo, S., Munchak, L.A., Remer, L.A., Sayer, A.M., Hsu, N.C., 2013. The Collection 6 MODIS aerosol products over land and ocean. Atmos. Meas. Tech. 6, 2989–3034. https://doi.org/10.5194/amtd-6-159-2013.

Li, T., Shen, H., Yuan, Q., Zhang, X., Zhang, L., 2017a. Estimating ground-level $PM_{2.5}$ by fusing satellite and station observations: a geo-intelligent deep learning approach. Geophys. Res. Lett. 44 (11) https://doi.org/10.1002/2017gl075710, 985-11,993.

Li, T., Shen, H., Zeng, C., Yuan, Q., 2020. A validation approach considering the uneven distribution of ground stations for satellite-based $PM_{2.5}$ estimation. IEEE J. Sel. Top. Appl. Earth Obs. Rem. Sens. 13, 1312–1321. https://doi.org/10.1109/jstars.2020.2977668.

Li, T., Shen, H., Zeng, C., Yuan, Q., Zhang, L., 2017b. Point-surface fusion of station measurements and satellite observations for mapping $PM_{2.5}$ distribution in China: methods and assessment. Atmos. Environ. Times 152, 477–489. https://doi.org/10.1016/j.atmosenv.2017.01.004.

Li, Z., Zhang, Y., Shao, J., Li, B., Hong, J., Liu, D., Li, D., Wei, P., Li, W., Li, L., Zhang, F., Guo, J., Deng, Q., Wang, B., Cui, C., Zhang, W., Wang, Z., Lv, Y., Xu, H., Chen, X., Li, L., Qie, L., 2016. Remote sensing of atmospheric particulate mass of dry $PM_{2.5}$ near the ground: method validation using ground-based measurements. Remote Sens. Environ. 173, 59–68. https://doi.org/10.1016/j.rse.2015.11.019.

Liu, J., Weng, F., Li, Z., 2019a. Satellite-based $PM_{2.5}$ estimation directly from reflectance at the top of the atmosphere using a machine learning algorithm. Atmos. Environ. 208, 113–122. https://doi.org/10.1016/j.atmosenv.2019.04.002.

Liu, J., Weng, F., Li, Z., Cribb, M.C., 2019b. Hourly $PM_{2.5}$ estimates from a geostationary satellite based on an ensemble learning algorithm and their spatiotemporal patterns over central east China. Rem. Sens. 11, 2120. https://doi.org/10.3390/rs11182120.

Ma, Z., Hu, X., Sayer, A.M., Levy, R., Zhang, Q., Xue, Y., Tong, S., Bi, J., Huang, L., Liu, Y., 2016. Satellite-based spatiotemporal trends in $PM_{2.5}$ concentrations: China, 2004-2013. Environ. Health Perspect. 124, 184–192. https://doi.org/10.1289/ehp.1409481.

Okuyama, A., Andou, A., Date, K., Hoasaka, K., Mori, N., Murata, H., Tabata, T., Takahashi, M., Yoshino, R., Bessho, K., 2015. Preliminary validation of Himawari-8/AHI navigation and calibration. In: Butler, J.J., Xiong, X., Gu, X. (Eds.), Earth Observing Systems Xx, p. 9607. https://doi.org/10.1117/12.2188978.

Peng, R.D., Bell, M.L., Geyh, A.S., McDermott, A., Zeger, S.L., Samet, J.M., Dominici, F., 2009. Emergency admissions for cardiovascular and respiratory diseases and the chemical composition of fine particle air pollution. Environ. Health Perspect. 117, 957–963. https://doi.org/10.1289/ehp.0800185.

Sarafian, R., Kloog, I., Just, A.C., Rosenblatt, J.D., 2019. Gaussian Markov random fields versus linear mixed models for satellite-based PM2.5 assessment: evidence from the northeastern USA. Atmos. Environ. 205, 30–35. https://doi.org/10.1016/j.atmosenv.2019.02.025.

Seinfeld, J.H., Bretherton, C., Carslaw, K.S., Coe, H., DeMott, P.J., Dunlea, E.J., Feingold, G., Ghan, S., Guenther, A.B., Kahn, R., Kraucunas, I., Kreidenweis, S.M., Molina, M.J., Nenes, A., Penner, J.E., Prather, K.A., Ramanathan, V., Ramaswamy, V., Rasch, P.J., Ravishankara, A.R., Rosenfeld, D., Stephens, G., Wood, R., 2016. Improving our fundamental understanding of the role of aerosol-cloud interactions in the climate system. Proc. Natl. Acad. Sci. U.S.A. 113, 5781–5790. https://doi.org/10.1073/pnas.1514043113.

Shen, H., Li, T., Yuan, Q., Zhang, L., 2018. Estimating regional ground-level $PM_{2.5}$ directly from satellite top-of-atmosphere reflectance using deep belief networks. J. Geophys. Res. Atmos. 123, 13875–13886. https://doi.org/10.1029/2018JD028759.

Singh, N., Murari, V., Kumar, M., Barman, S.C., Banerjee, T., 2017. Fine particulates over South Asia: review and meta-analysis of $PM_{2.5}$ source apportionment through receptor model. Environ. Pollut. 223, 121–136. https://doi.org/10.1016/j.envpol.2016.12.071.

Song, W.Z., Jia, H.F., Huang, J.F., Zhang, Y.Y., 2014. A satellite-based geographically weighted regression model for regional $PM_{2.5}$ estimation over the Pearl River Delta region in China. Remote Sens. Environ. 154, 1–7. https://doi.org/10.1016/j.rse.2014.08.008.

Song, Y., Huang, B., He, Q., Chen, B., Mahmood, R., 2019a. Dynamic assessment of $PM_{2.5}$ exposure and health risk using remote sensing and geo-spatial big data. Environ. Pollut. 253, 288–296. https://doi.org/10.1016/j.envpol.2019.06.057.

Song, Z.J., Fu, D.S., Zhang, X.L., Han, X.L., Song, J.J., Zhang, J.Q., Wang, J., Xia, X.G., 2019b. MODIS AOD sampling rate and its effect on $PM_{2.5}$ estimation in North China. Atmos. Environ. 209, 14–22. https://doi.org/10.1016/j.atmosenv.2019.04.020.

Sorek-Hamer, M., Broday, D.M., Chatfield, R., Esswein, R., Stafoggia, M., Lepeule, J., Lyapustin, A., Kloog, I., 2017. Monthly analysis of PM ratio characteristics and its relation to AOD. J. Air Waste Manag. Assoc. 67, 27–38. https://doi.org/10.1080/10962247.2016.1208121.

Sun, J., Gong, J.H., Zhou, J.P., 2021. Estimating hourly $PM_{2.5}$ concentrations in Beijing with satellite aerosol optical depth and a random forest approach. Sci. Total Environ. 762 https://doi.org/10.1016/j.scitotenv.2020.144502.

Sun, L., Wei, J., Duan, D.H., Guo, Y.M., Yang, D.X., Jia, C., Mi, X.T., 2016. Impact of Land-Use and Land-Cover Change on urban air quality in representative cities of China. J. Atmos. Sol. Terr. Phys. 142, 43–54. https://doi.org/10.1016/j.jastp.2016.02.022.

Vu, B.N., Sanchez, O., Bi, J.Z., Xiao, Q.Y., Hansel, N.N., Checkley, W., Gonzales, G.F., Steenland, K., Liu, Y., 2019. Developing an advanced $PM_{2.5}$ exposure model in Lima, Peru. Rem. Sens. 11 https://doi.org/10.3390/rs11060641.

Wang, B., Yuan, Q., Yang, Q., Zhu, L., Li, T., Zhang, L., 2021. Estimate hourly $PM_{2.5}$ concentrations from Himawari-8 TOA reflectance directly using geo-intelligent long short-term memory network. Environ. Pollut. 271, 116327 https://doi.org/10.1016/j.envpol.2020.116327.

Wang, Y., Yuan, Q.Q., Li, T.W., Shen, H.F., Zheng, L., Zhang, L.P., 2019. Large-scale MODIS AOD products recovery: spatial-temporal hybrid fusion considering aerosol variation mitigation. ISPRS J. Photogrammetry Remote Sens. 157, 1–12. https://doi.org/10.1016/j.isprsjprs.2019.08.017.

Xue, T., Zheng, Y.X., Tong, D., Zheng, B., Li, X., Zhu, T., Zhang, Q., 2019. Spatiotemporal continuous estimates of $PM_{2.5}$ concentrations in China, 2000-2016: a machine learning method with inputs from satellites, chemical transport model, and ground observations. Environ. Int. 123, 345–357. https://doi.org/10.1016/j.envint.2018.11.075.

Yang, J., Guo, Q., Lu, F., Wei, C., Zhang, Z., 2017. Introducing the new generation of Chinese geostationary weather satellites, Fengyun-4. Bull. Am. Meteorol. Soc. 98, 1637–1658. https://doi.org/10.1175/bams-d-16-0065.1.

Yang, Q., Yuan, Q., Yue, L., Li, T., Shen, H., Zhang, L., 2019. The relationships between $PM_{2.5}$ and aerosol optical depth (AOD) in mainland China: about and behind the

spatio-temporal variations. Environ. Pollut. 248, 526–535. https://doi.org/10.1016/j.envpol.2019.02.071.

Yu, W., Liu, Y., Ma, Z., Bi, J., 2017. Improving satellite-based $PM_{2.5}$ estimates in China using Gaussian processes modeling in a Bayesian hierarchical setting. Sci. Rep. 7 https://doi.org/10.1038/s41598-017-07478-0.

Zou, B., Pu, Q., Bilal, M., Weng, Q., Zhai, L., Nichol, J.E., 2016. High-resolution satellite mapping of fine particulates based on geographically weighted regression. Geosci. Rem. Sens. Lett. IEEE 13, 495–499. https://doi.org/10.1109/lgrs.2016.2520480.